Computerized Medical Imaging and Graphics 36 (2012) 591–600

Contents lists available at SciVerse ScienceDirect

Computerized Medical Imaging and Graphics

journal homepage: www.elsevier.com/locate/compmedimag

Automatic brain caudate nuclei segmentation and classification in diagnostic of Attention-Deficit/Hyperactivity Disorder

Laura Igual[a,b,*], Joan Carles Soliva[c,1], Sergio Escalera[a,b,2], Roger Gimeno[a,3], Oscar Vilarroya[c,1], Petia Radeva[a,b,4]

[a] Dept. Applied Mathematics and Analysis, Universitat de Barcelona, Gran Via Corts Catalanes 585, 08007 Barcelona, Spain
[b] Computer Vision Center, Campus UAB, Building O, 08193 Bellaterra, Barcelona, Spain
[c] Unitat de Recerca en Neurociència Cognitiva, Dept. of Psychiatry, Universitat Autònoma de Barcelona and Fundació IMIM, Spain

ARTICLE INFO

Article history:
Received 3 March 2012
Received in revised form 11 July 2012
Accepted 13 August 2012

Keywords:
Automatic caudate segmentation
Attention-Deficit/Hyperactivity Disorder
Diagnostic test
Machine learning
Decision stumps
Dissociated dipoles

ABSTRACT

We present a fully automatic diagnostic imaging test for Attention-Deficit/Hyperactivity Disorder diagnosis assistance based on previously found evidences of caudate nucleus volumetric abnormalities. The proposed method consists of different steps: a new automatic method for external and internal segmentation of caudate based on Machine Learning methodologies; the definition of a set of new volume relation features, 3D Dissociated Dipoles, used for caudate representation and classification. We separately validate the contributions using real data from a pediatric population and show precise internal caudate segmentation and discrimination power of the diagnostic test, showing significant performance improvements in comparison to other state-of-the-art methods.

1. Introduction

Attention-Deficit/Hyperactivity Disorder is a developmental disorder characterized by inattentiveness, motor hyperactivity, and impulsiveness, which represents the most prevalent psychiatric disorder in childhood [1]. It is estimated that half of children with ADHD will display the disorder in adulthood. Given its prevalence and pervasiveness, ADHD imposes an enormous burden on families and society in terms of the number of people afflicted and the possible associated economic losses. Moreover, there are contradictory studies pointing to overdiagnosis, underdiagnosis, and undertreatment of ADHD, which incited the debate about the difficulty of the ADHD diagnosis [2]. These facts, together with the fast-growing use of neuroimaging techniques in ADHD research, have prompted an inquiry into the feasibility of an imaging test for the diagnosis of ADHD that could represent substantial aid in clinical practice [3].

The structural MRI has provided fairly consistent ground research in the pediatric ADHD population. See [3] for a more extensive review. In particular, the decreased volume of the right caudate nucleus seems to be reasonably replicated across different pediatric ADHD samples [4–11]. Studies in [11,12] were conducted with male and female ADHD participants. Moreover, volumetric differences on the body of the right caudate nucleus have been found to be significant in ADHD and control groups [4,6]. Drawing on this finding, the authors of [13] proposed a diagnostic imaging test that appears to achieve all purposes of the phases I (ground research) and II (assessment of clinical adequacy) of the multiphase approach for developing a diagnostic imaging test [14,3]. Given its good accuracy, it could be considered as a promising ancillary diagnostic tool to rule out an ADHD diagnosis in the pediatric population. However, the clinical implementation of this diagnostic test suffers from two main drawbacks. On one hand, it lacks an appropriate and objective segmentation system, and thus, requires experts to manually segment the involved brain structures on a slice-by-slice basis. In the case of caudate nuclei, besides the external segmentation, which consists in the delineation of the structure external boundaries, internal caudate segmentation is necessary to separately examine the head and body areas. Thus, the manual segmentation process is extremely time consuming, and prone to inter-rater discrepancies, limiting the power of the presented diagnostic strategy. In order to

* Corresponding author at: Dept. Applied Mathematics and Analysis, Universitat de Barcelona, Gran Via Corts Catalanes 585, 08007 Barcelona, Spain.
Tel.: +34 93 4020854; fax: +34 93 4021601.
E-mail addresses: ligual@ub.edu (L. Igual), 24744jsv@comb.cat (J.C. Soliva), sergio@maia.ub.es (S. Escalera), rogergimenohernandez@gmail.com (R. Gimeno), oscar.vilarroya@gmail.com (O. Vilarroya), petia@cvc.uab.es (P. Radeva).
[1] Tel.: +34 93 3160485; fax: +34 93 3160410.
[2] Tel.: +34 93 4020853; fax: +34 93 4021601.
[3] Tel.: +34 93 5942473; fax: +34 93 5942479.
[4] Tel.: +34 93 4020852; fax: +34 93 4021601.

0895-6111/$ – see front matter © 2012 Elsevier Ltd. All rights reserved.
http://dx.doi.org/10.1016/j.compmedimag.2012.08.002

accelerate the required caudate analysis and make the procedure feasible for large amount of data, an automatic approach is necessary. Nowadays, automatic external segmentation of subcortical structures in the brain is an active line of research, and acceptable solutions can be found. However, to our knowledge, there is not any method in the literature for automatic internal segmentation of the caudate. On the other hand, the proposed diagnostic test [13] is based on the ratio between right caudate body volume (rCBV) and the total bilateral caudate body volume (bCBV). Thus, the method is limited to the discriminative power of this measure with the delicate operation of defining a threshold for it. Instead, new volumetric shape descriptors could be exploited to include morphometric information and improve final classification.

The main objective of this work is to define a unique completely automatic system for ADHD diagnostic test inspired by [13]. First, we obtain a globally optimal external segmentation of the caudate in an MRI applying the recently proposed CaudateCut approach [15]. We propose a new automatic internal segmentation to separate caudate head and body areas, learning a classifier based on an extended set of shape features describing the caudate region at each slice. As a result, we consider head and body volumes separately and define a set of new volumetric features, named 3D Dissociated Dipoles, describing relations between caudate head and body areas. Finally, we build an automatic diagnostic test by learning a Machine Learning classifier based on these caudate volumetric features. In the experiments, we compare the results obtained by our new fully-automatic method with those obtained by the manual procedure provided in [13] and state-of-the-art feature descriptors on real data with ADHD and control subjects. As a result, we show accurate internal caudate segmentation and comparable results obtained by the proposed automatic diagnostic test with respect to this manual strategy, obtaining significant performance improvement in the diagnostic test in comparison to classic approaches.

The rest of the paper is organized as follows: Section 2 reviews the related state-of-the-art work. Section 3 introduces the method of automatic ADHD diagnostic test, detailing the internal caudate segmentation and automatic diagnostic test. Section 4 explains the considered material and validation protocol and shows the experimental results. Section 5 presents the discussion, and, finally, Section 6 concludes the paper.

2. Related work

An increasing number of research works focused on automatic techniques for studying brain region atrophy in application to Alzheimer's disease [16–21]. Likewise, some works have been presented related to the predictive power of MRI in autism [22,23] and depression [24,25]. On the contrary, no works have been presented on ADHD in this direction.

Different methods can be exploited to extract the geometric information necessary for a useful statistical study in separating two populations (healthy and non-healthy people) [26]. Classic approaches evaluate volumetric variations to explain atrophy due to such kinds of illnesses [27]. Some state-of-the-art methods focused on detecting brain morphological abnormalities are based on useful shape descriptors. In [28] authors proposed a shape analysis of lateral ventricles by parameterizing their surfaces and described them using spherical harmonics. In [29], the authors propose an anatomical pattern discovery technique for learning features which can potentially be image biomarkers of diseases. Other classes of methods have been introduced for generic object analysis employing heat diffusion procedures on 3D shapes [30,31]. In [32], 3D Haar-like features were used to encode context in brain tissue classification. In [26], several local tissue volumetric measurements were computed and some of them were selected using Support Vector Machines (SVM) for classification of structural brain MRI. The list of references included here is by no means exhaustive. We do not intend to present a full review of existing techniques, but to present the current context and discuss a set of works that are representative of the diversity of the proposed approaches for feature extraction. Despite the large amount of existing techniques, our target structure, the caudate nucleus, is a small structure and many of these descriptors are not useful for its representation.

3. Method

We propose a method that is split into three main steps: (1) external caudate segmentation, (2) internal caudate segmentation based on shape features, and (3) ADHD diagnostic test based on extended volumetric features. Fig. 1 shows the method pipeline. Step 1 is performed using the recently proposed CaudateCut segmentation algorithm [15] specially conceived for the caudate boundary delineating in MRI slices. CaudateCut integrates an atlas-based segmentation strategy with an Graph Cut (GC) energy-minimization framework [33]. The GC model is specially adapted to make it suitable for segmenting small, low-contrast structures, such as the caudate nucleus, by defining new energy function data and boundary potentials. In particular, information concerning the intensity and geometry is exploited and supervised energies are added based on contextual brain structures. Boundary detection using a new multi-scale edgeness measure is also introduced. It is important to note that all of this system is fully-automatic, including the initial definition of seeds, so no human intervention is needed to choose these seeds. Steps 2 and 3 represent the contribution of this paper and are described in the next subsections.

3.1. Internal segmentation: head and body separation

Given the external segmentation of the caudate nuclei in MRI slices, it is necessary to distinguish the images of Region Of Interest (ROI) corresponding to the caudate head from those corresponding to the caudate body for further application of diagnostic testing. We use information a priori of the caudate shape in axial views of MRI volumes. Caudate head structure tends to be wider, while the body tends to be elongated. An example of head and body caudate regions are shown in Fig. 2(a)–(c). Moreover, first caudate slices in the axial projection of the MRI volumes always correspond to the head and the final to the body.

We propose two different strategies to perform the internal segmentation. Both methods are based on internal landmarks and thus, avoid localizing the caudate's neighbor structures used as external references. First, we present an automatic method implementing the geometric criterion analysis proposed in [4] by using Computer Vision techniques. Second, we use new shape features and SVM to learn a classifier able to recognize head and body ROI shapes. Finally, we apply a postprocessing step based on Decision Stumps to filter the slice classification and improve the final classification.

3.1.1. Automatic geometric criterion

Authors in [4] define the following geometric criteria according to which the caudate head or body ROIs fulfill the following inequalities in the general cases:

$$\frac{h(H)}{w(H)} \leq 2, \quad \frac{h(B)}{w(B)} > 2, \tag{1}$$

where H and B denote head and body ROIs, and h and w are the height and width of the ROI, respectively. The underlying idea of these geometric criteria is relatively intuitive and the automation

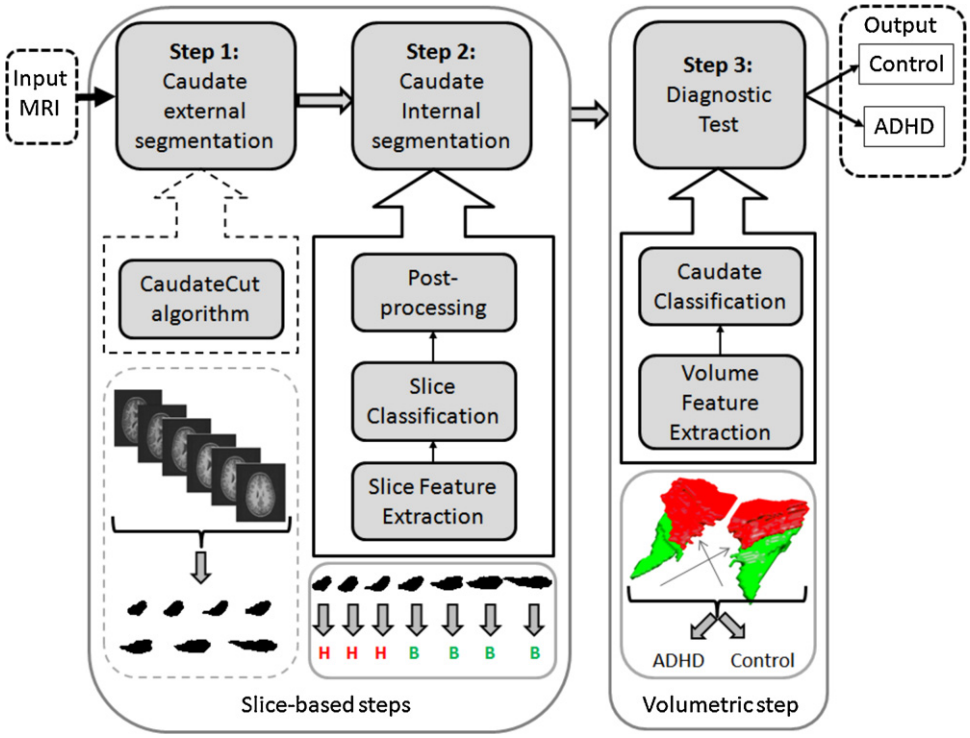

Fig. 1. Overview of the proposed fully automatic diagnostic test pipeline.

is simple. We follow the next steps: first, the MRI volumes must be oriented in the AC-PC line [34]. Second, the MRI caudate slices with ROI whose bounding box area is lower than a threshold T_area are discarded in order to avoid noisy regions. Then, the two larger horizontal and vertical lines within the ROI are computed (Fig. 2(b)–(d)). Finally, the geometric criterion is directly applied using the length of these two lines (in pixels) and the slice is classified as head or body.

One of the main problems with this strategy is the small range of values the relation h/w takes. For most of the images, these relations take values near the threshold, 2, defined in Eq. (1). This proximity to the threshold implies difficulties in the definition of the border between head and body slices. Thus, in the final classification, images belonging to different parts of the caudate appear mixed. An example of the ROI classification can be seen in Fig. 3(a), where the second image of the sequence is incorrect. This result is not in accordance with the condition in which the first caudate images correspond to the caudate head and the last ones to the caudate body, and they are not mixed. In order to avoid these kinds of errors, a post processing method based on the a priori knowledge of the problem is applied. This post-process is explained in the following sections.

3.1.2. Learning shapes

In order to improve internal caudate segmentation, we propose an alternative method based on the extraction of an extended set of shape features describing the caudate region for each slice and their classification using SVM. The set of features are composed of the following properties of the ROI: ROI area, ratio between height and width of the ROI, height, width and area of the bounding box containing the ROI, extent (ratio of pixels in the ROI and pixels in the total bounding box), major and minor axis length of the ellipse that has the same normalized second central moments as the ROI, orientation of the ellipse, eccentricity (ratio of the distance between the foci of the ellipse and its major axis length), perimeters ratio (relation between the perimeter of the circle with the same area as the ROI, and the perimeter of the ROI), and x and y coordinates of the ROI centroid. See Fig. 3(b) for an illustration of a ROI and its bounding box (red), ellipse (blue), and centroid (orange). Once we compute the set of features of the caudate regions for all the slices

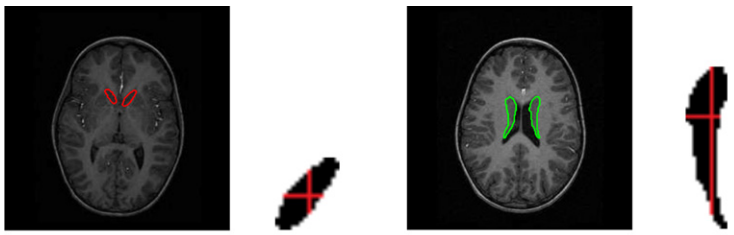

Fig. 2. Example of (a) caudate head image, and (c) caudate body image, with caudate nuclei marked in red and green, respectively. Examples of (b) head ROI and (d) body ROI with the two larger horizontal and vertical lines depicted. (For interpretation of the references to color in this figure legend, the reader is referred to the web version of the article.)

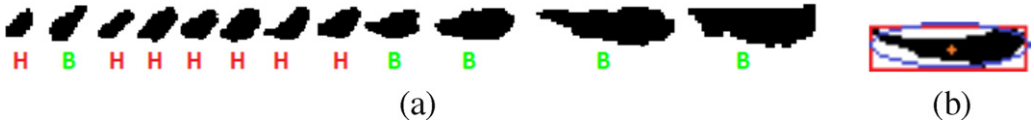

Fig. 3. (a) Example of images classified as head (H) and body (B) images. (b) Example of a ROI with its bounding box (red), ellipse (blue), and centroid (orange). (For interpretation of the references to color in this figure legend, the reader is referred to the web version of the article.)

we use SVM classifier to build a system able to classify head and body caudate regions.

3.1.3. Post-processing

Decision stump (DS) is a machine learning model that consists of one-level decision tree [35]. That means the system is configured as the root node which is immediately connected to the terminal nodes. A DS makes a polarity prediction based on the value of just a single input feature. When the DS works on continuous features, usually a threshold feature value is selected, and the stump contains two leaves (for values below and above the threshold). DS is often used as a weak classifier [36] in machine learning ensemble techniques such as bagging and boosting. Here, we apply DS to find a unique separation between caudate head and body images and obtain a homogeneous classification. Thus, images classified as head in the middle of body sections, or vice versa, are relabeled.

The procedure is the following. The error weight for each class is set to 1 divided by the number of occurrences for each class:

$$\omega_e(Head) = \frac{1}{\#Head\ images}$$

$$\omega_e(Body) = \frac{1}{\#Body\ images}$$

A loss function, F_x, describing the importance in the order of appearance of head or body images is defined for each class. Previous analysis says that the disposition of the samples is the following: between 60 and 70% of the MRI caudate slices for each subject corresponds to the caudate head, while 30–40% are from the caudate body. For this reason, the downfall curve that represents each class (head and body) along all the slice positions in the classification is defined in a different way. In the head class, the drop curve is set as linear:

$$F_x(Head) = \frac{1 - iCounter}{num\ Elements},$$

while for the body, two cases are studied, quadratic and cubic slope:

$$F_x(Body) = \frac{iCounter^d}{num\ Elements^d}, \quad d = \{2, 3\}$$

Fig. 4 illustrates the loss functions for head (linear) and body (cubic). In this way, we strongly penalize the apparition of body regions in the first positions. Once the weight and loss function are defined, the system search for the optimal division between caudate head and body sections in terms of error, computing it as $\omega_e \cdot F_x$. The position giving the smallest error is selected as the separation position and the images are consequently relabeled. After applying DS, the non-homogeneous classifications disappeared, and the global classification can be, in consequence, improved. Fig. 5 shows two examples of classification improvements using DS. Note that in the second case, even if there is an improvement, the result is not perfect compared to the GT data.

3.2. Diagnostic test

The objective of the diagnostic test is to classify MRI volumes as corresponding to ADHD and control subjects. In [13], authors

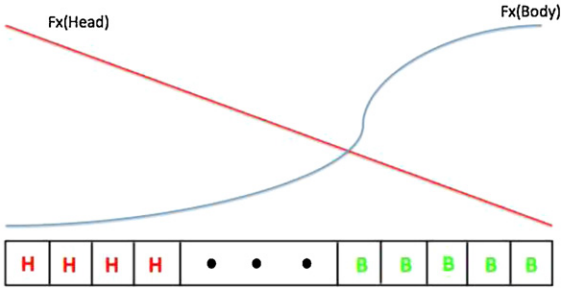

Fig. 4. Loss response function for each class (head and body).

presented a diagnostic test to assist in the diagnosis of ADHD in children based on the ratio

$$r_0 = \frac{rCBV}{bCBV}. \tag{2}$$

Using the Receiver Operating Characteristic (ROC) curve analysis on this ratio, the Optimal Cut-Off Value (OCOV) is estimated as the optimal ratio for which the specificity is greater or equal to a threshold Th_{spec}, and can be applied to classify new subjects.

The previous diagnostic test synthesizes the group caudate differences in one ratio value and performs decision with it. Contrarily, we look for useful morphometric features of the caudate which could amplify these group differences. We introduce a simple but efficient region-based feature representation and learn the optimal frontier between ADHD and control groups using a machine learning approach. Based on the internal segmentation of the caudate nucleus, we extend the feature set using volume relations between parts of caudate head and body. In particular, our feature description methodology is inspired by the Haar-like feature representation and the generalized set of features named Dissociated Dipoles [37,38]. Haar-like features are biologically inspired features characterized by computational simplicity: for each voxel, it is possible to extract a value obtained by the weighted sum of the intensities on the area spanned by a template, with the sum of the weights being zero. There are many types of templates, usually dense blocks of various sizes and subdivisions oriented along three dimensions. Haar-like features have already been successfully used in the field of computational vision [39], where they usually come along with a robust method of supervised classification. The Haar-like features have been recently extended to be computed in 3D volumes and used in several MRI applications [40,32,41]. On the other hand, Dissociated Dipoles [38] generalize Haar-like features by including non-local comparisons. Dissociated Dipoles representation allows the computation of feature relations from non-contiguous blocks, being that the Haar-like features a particular subset. In this work, we propose and use the new 3D Dissociated Dipoles to measure the volume relations among a set of 3D caudate blobs. These volume relations are strategically defined among the caudate head and body segmented regions. In particular, we proceed as follows: given volumetric right and left head H_i^r, H_i^l and body B_i^r, B_i^l regions for subject i, we split each H_i and B_i volume in two height equidistant volumes, H_{ij} and B_{ij}, $\forall j \in \{1, 2\}$, and compute all pairs of volume relations without repetitions, which

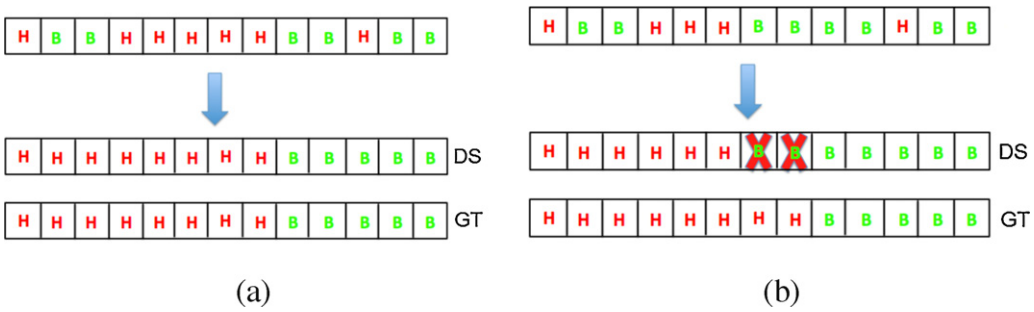

Fig. 5. Two examples of the Decision Stumps performance. In (a), DS works correctly and give the result as in the Ground Truth (GT) In (b), DS does not works correctly compared with the GT.

results in 7 + 6 + 5 + 4 + 3 + 2 + 1 = 28 relations. The volume relations for subject i can be formally defined as follows:

$$r_{ij} = \left\{ \frac{\mathrm{vol}(\mathcal{H}^{l}_{ij})}{\mathrm{vol}(\mathcal{B}^{k}_{im})} \right\}_{j,m\in\{1,2\},k\in\{l,r\},\mathcal{H},\mathcal{B}\in\{H,B\}} , \{\mathcal{H}, j, l\} \neq \{\mathcal{B}, m, k\}. \quad (3)$$

where vol(·) represents the absolute volume in voxels of the corresponding 3D region defined by the argument '·'. Thus, the set of 3D Dissociated Dipoles features r_{ij} together with the previously defined ratio, r_0, form a final feature vector of 29 elements for each subject. An illustrative example of the feature regions for a given segmented left and right head (red) and body (green) caudate regions are shown in Fig. 6. Moreover, in the case that the number of considered features and volumes was larger, the proposed feature set can be efficiently computed using an integral image representation [42]. Then, we learn a binary ADHD diagnostic test classifier using SVM.

4. Experiments and results

In this section, we present the experiments and results obtained for caudate segmentation and classification. Before presenting the results, we first describe the considered database, the methods of the comparison and the validation protocol. Then, we detail the obtained results for (1) the caudate segmentation, as well as its comparison with a standard approach, (2) evaluate the new automatic ADHD diagnostic test, and (3) compare it with the manual strategy and other state-of-the-art methods for significant analysis.

4.1. Image database

URNC database includes 39 children (35 boys and 4 girls) with ADHD, according to DSM-IV, referred from the Unit of Child Psychiatry at the Vall d'Hebron Hospital in Barcelona, Spain, and coordinated by the Unit of Research in Cognitive Neuroscience (URNC) at the IMIM Foundation, together with 39 control subjects (27 boys and 12 girls) recruited from the community. The mean age of the groups was 10.8 (SD: 2.9) and 11.7 (SD: 3), respectively. The groups were matched for handedness and IQ. All subjects underwent a MRI examination with a 1.5 T system (Signa, General Electric, Milwaukee, WI, USA). We performed a volumetric fast spoiled gradient (FSPGR-T1 3D) axial sequence (TR = 13.2 ms; TE = 4.2 ms; FA = 15; NEX = 1; 256 × 256 matrix), with 2-mm partitions, and a dual-echo fast spin echo (FSE-DP-T2) axial sequence (TR = 3980 ms; TE = 20/100 ms; NEX = 2; 512 × 512 matrix), with 5-mm sections and a 2-mm gap.

Children with ADHD received a consensus diagnosis by an expert team. Moreover, expert annotations of the 79 individual caudate nuclei were obtained. In particular, slice by slice manual annotation of external caudate boundaries and caudate regions identification (head and body) were performed following the procedure described in [4]. MRIcro software[5] was used for volume labeling and manipulation. Taking these annotations as Ground Truth (GT), we have three GT sets at two different levels available: the external and internal caudate nucleus segmentations at the slice level, and ADHD positive or negative diagnosis at the subject level.

4.2. Comparison methods

We compare the proposed methods for caudate internal segmentation and diagnostic test with the state-of-the-art methods enumerated in the following. All the methods are developed using Matlab 7.7.0 [6] and the matlab toolbox *libsvm* [7] is used for the SVM classification.

4.2.1. Caudate internal segmentation

- *Geometric criterion.* Automatic method implementing the geometric criterion described in Section 3.1. The threshold T_{area} is set empirically to 50 pixels.
- *Shape-based classification.* Automatic method based on the new set of slice shape features and the SVM classifier approach presented in Section 3.1. The parameters of the SVM are set empirically by cross-validation.

4.2.2. Diagnostic test

- *Ratio ROC method.* ROC-based diagnostic strategy proposed in [13] based on ratio r_0 (Eq. (2)). *Manual ratio* stands for the manually computation of the ratio using manual external and internal segmentations of caudate nuclei. *Auto ratio* means that the computation of the ratio uses the results of the automatic shape-based classification of caudate ROI images previously segmented by CaudateCut method.
- *GHKS method.* Diagnostic tests using Global Heat Kernel Signature (GHKS) feature extraction method [30] and a classification technique. GHKS feature extraction method is implemented as described in [30] with the following parameters: number of eigenvalues 200, number of bins 10, range of the scale-space is defined by 400 logarithmically equally spaced points between log(0.00001)/log(10) and log(500,000)/log(10).
- *GDD method.* Diagnostic tests using Global Dissociated Dipoles (GDD) and a classification technique. GDD are defined dividing the caudate structure in four equidistant volumes, without considering the caudate head and body areas. GDD can be seen as a simplification of the proposed Dissociated Dipoles features.

[5] www.cabiatl.com/mricro/.
[6] Code of all the methods are public upon to request to the authors of the paper.
[7] www.csie.ntu.edu.tw/cjlin/libsvm/.

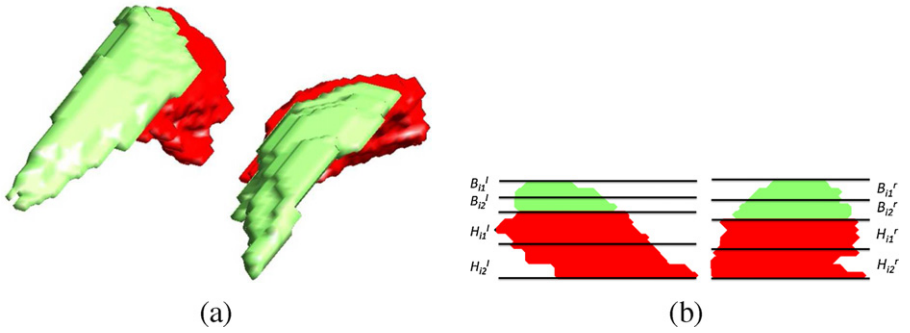

Fig. 6. (a) Example of 3D automatic segmented caudate regions (head in red and body in green, respectively). (b) Defined regions to compute the extended feature set for posterior diagnostic test. (For interpretation of the references to color in this figure legend, the reader is referred to the web version of the article.)

- *ADA method.* Our Automatic Diagnostic of ADHD (ADA) method introduced in Section 3.2 based on the proposed 3D Dissociated Dipoles (DD) features and a classification technique.

In all these methods, two state-of-the-art Machine Learning classifiers, Real Adaboost [43] and SVM, are considered and their parameters are set empirically (see next section).

4.3. Validation protocol

We compute the following three measures based on True Positive (TP), False Positive (FP), True Negative (TN) and False Negative (FN):

$$\text{Accuracy} = \frac{(TP+TN)}{(TP+TN+FP+FN)},$$

$$\text{Sensitivity} = \frac{TP}{(TP+FN)},$$

$$\text{Specificity} = \frac{TN}{(TN+FP)}$$

In the internal caudate segmentation validation, the head label corresponds to positive and the body label to negative. In the diagnostic test validation, ADHD patients correspond to positive and control subjects to negative.

In all the experiments we use 5-fold cross-validation as a validation strategy. For the internal segmentation we divide into 5 subsets the set of 1039 caudate images from the 78 subjects. Moreover, note that for each fold, none of the subjects in the test set is present in the training set. This strategy can obtain equal or more significantly results than other strategies [44]. In the ratio ROC method, for each fold, we performed a ROC curve analysis using the training set to learn the OCOV as the optimal ratio threshold where the specificity was greater or equal than 85%, and test this OCOV on the test set of each 5-fold. Finally, we compute the mean accuracy, sensitivity and specificity of the five folds.

Finally, Adaboost and Support Vector Machine classifiers are used as the different classification strategies for the different experiments. For Adaboost, we use 100 decision stumps as the base classifier. In order to train RBF and Polynomial SVM, 5-fold cross validation was used. For RBF SVM we tune the γ parameter in the range $[0, \ldots, 1]$ with increments of 0.001, saving a 10% of the training data of each fold to validate the generalization capability of each tuned kernel parameter.

For a statistical test, we consider the rankings obtained estimating each particular ranking r_i^j for each data sequence i and each system configuration j, and computing the mean ranking R for each configuration as $R_j = (1/N)\sum_i r_i^j$, where N is the total number of measurements. In order to reject the null hypothesis that the measured ranks differ from the mean rank, and that the ranks are affected by randomness in the results, we use the Friedman test [45]. The Friedman statistic value is computed as follows:

$$X_F^2 = \frac{12N}{k(k+1)}\left[\sum_j R_j^2 - \frac{k(k+1)^2}{4}\right], \tag{4}$$

where k is the number of methods in the comparative.

Since this value X_F^2 is undesirably conservative, Iman and Davenport [46] proposed a corrected statistic:

$$F_F = \frac{(N-1)X_F^2}{N(k-1)-X_F^2}. \tag{5}$$

Once we have checked for the non-randomness of the results, we can perform an a post-hoc test to check if one of the configurations can be statistically singled out. For this purpose we use the Nemenyi test [45]. The Nemenyi statistic is obtained as follows:

$$CD = q_\alpha \sqrt{\frac{k(k+1)}{6N}}. \tag{6}$$

4.4. Caudate nuclei segmentation results

External segmentation. Details on the validation of CaudateCut method can be found in [15], where it is reported that it obtain volumetric mean overlap of 82.60% on the URNC data.

Internal segmentation. In order to evaluate the two proposed methods for internal segmentation, we use 5-fold cross validation strategy over the set of caudate ROI images externally segmented by CaudateCut method. In Fig. 7, we summarize the comparative among geometric criterion and shape-based classification strategies in terms of accuracy, sensitivity and specificity. All the methods obtain accuracies over 91%, but the shape-based strategies with DS application stand out when paying close attention to accuracy values. In particular, the best strategy is the shape-based classification using linear SVM with cubic DS. This strategy achieves accuracy, sensitivity and specificity of 94.04%, 96.21% and 91.23%, respectively. Moreover, in Fig. 7, it is possible to appreciate the benefit of using DS for all methods. Nevertheless, the improvement obtained by DS application is higher for shape-based classification strategies than for geometric criterion. One of the main causes of the failure of the automatic geometric criterion was the small range of values in the criterion. For this reason, this method introduces many false detections, alternating head and body labels in the first classification result. This misleads the subsequent application of DS for finding the best boundary and makes this method less useful in this case.

In regards to sensitivity and specificity results, note that, in all cases, the sensitivity is higher than the specificity, meaning that

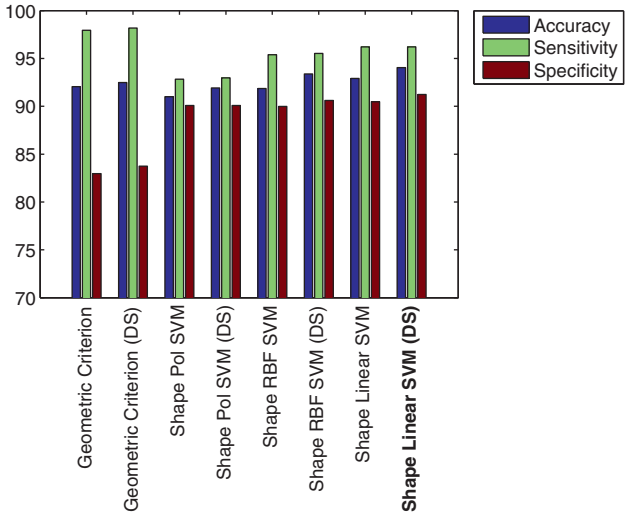

Fig. 7. Comparative (in terms of accuracy, sensitivity and specificity) of internal segmentation strategies: geometric criterion and shape-based classification with different SVM kernels (linear, polynomial and RBF), and without and with DS application. The best result is obtained by the shape-based classification with Linear SVM and DS achieving 94.04% accuracy.

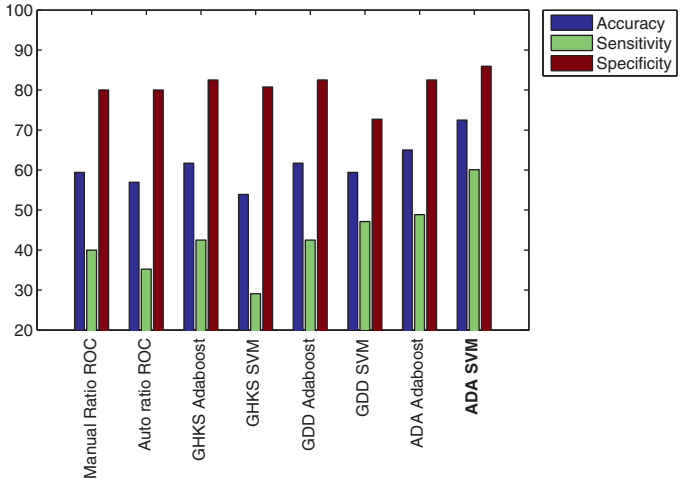

Fig. 9. Comparison of the diagnostic test strategies. Mean accuracy, sensitivity and specificity of the 5-fold validation for 7 different strategies: ROC-based diagnostic procedure with manual ratio, GHKS, GDD and ADA methods with Adaboost and SVM classifiers. Full details can be found in Section 4.2. The highest classification performance (accuracy 72.48%, specificity of 85.93% and sensitivity of 60.07%) is obtained by ADA SVM (column 8).

head ROI images are better detected than the ones corresponding to body images. These kinds of results were what we expected for the strategies based on SVM classifier, since the classification problem is, by definition, unbalanced (the number of head images is approximately 20% greater than the number of body images in the training set). Besides, analyzing the geometric criterium performance with DS, we observed that this method tends to define a head area larger than it was manually defined in the GT.

In Fig. 8, we show qualitative results of the classification of the automatic shape-based method with the best classifier (Linear SVM). It can be seen that head and body ROIs have coincident characteristics intragroup and differences intergroup. It is important to emphasize that after DS application the remaining errors are placed near the boundary separating the head and body parts.

4.5. Diagnostic test results

In this section, we validate the discriminative power of the proposed ADA method to differentiate between control and ADHD subjects. We compare it with state-of-the-art methods and the manual method. Concretely, we evaluate the new extended DD features used to represent the data, as well as the classification strategy (real Adaboost and SVM with RBF kernel). For this, we perform 5-fold cross-validation, where for each fold, none of the subjects in the test set is present in the training set.

Fig. 9 summarizes the results of the validation experiments using automatic segmentations of the caudate nucleus. We compare the following strategies: ROC-based diagnostic procedure using ratio r_0, GHKS, GDD and ADA methods with SVM and Adaboost classifiers. The results of the methods are in terms of accuracy, sensitivity and specificity. From these results, it can be inferred that ADA method with SVM improves the rest of the strategies in accuracy, sensitivity and specificity. The proposed strategy achieved accuracy of 72.48%, specificity of 85.93% and sensitivity of 60.07%. The results are improved with respect to ratio-based methods, which implies not only, that this classifier offers better performance than the rest, but also that the new DD features offer more information than the ratio itself, improving the discrimination power in the final ADHD diagnostic test. Moreover, none of GHKS and GDD methods define features able to capture the group differences as well as ADA.

4.6. Significant analysis results

In order to deeply analyze the significance of the performances provided for each of theses 8 strategies (manual ratio, automatic ratio, GHKS SVM, GHKS Adaboost, GDD SVM, GDD Adaboost, ADA SVM and ADA Adaboost), we performed a statistical test to compare them. Fig. 10 shows the mean rank for each strategy considering the six measurements: accuracy, sensitivity and specificity for the manual and automatic strategies. The rankings were obtained as explained in Section 4.3. Note that for convenience of the experiment, we considered diagnostic methods using manual and automatic caudate segmentations versions of the same strategy. For

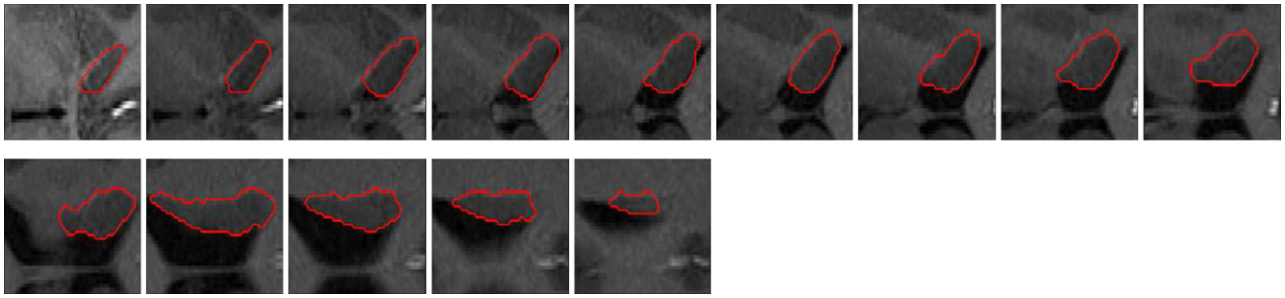

Fig. 8. Qualitative results of internal caudate segmentation. ROIs classified as head (first row) and body (second row) by the automatic system. The last image in the first row represents an error, since it corresponds to a body slice in the GT.

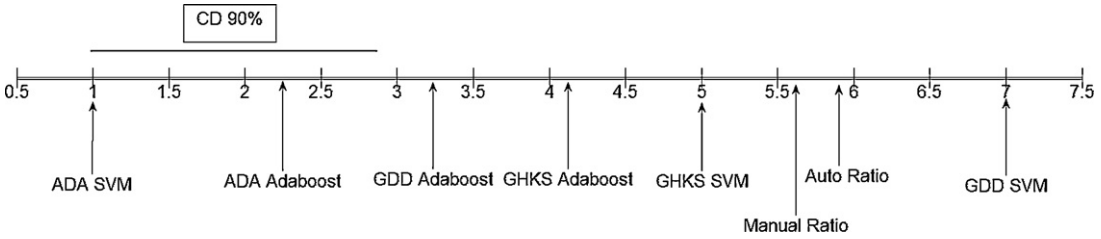

Fig. 10. Nemenyi test result for the 8 methods. The critical value for 90% of confidence is $CD = 1.83$.

reading Fig. 10, note that a lower value in the depicted axis signifies a better performance of the method.

We compute the Friedman statistic value, as described in Section 4.3, with $k = 8$ system configurations to compare, and obtain $X_F^2 = 13.06$. Since this value is undesirably conservative, we compute the corrected statistic and we obtain $F_F = 2.28$. With 8 configurations and 6 measurements, F_F is distributed according to the F distribution with 7 and 35 degrees of freedom. The critical value of $F(7, 35)$ for 0.05 is 2.24. As the value of $F_F = 2.28$ is higher than 2.24 we can reject the null hypothesis.

Moreover, we perform a post hoc test to check if one of the configurations can be statistically singled out. For this purpose we use the Nemenyi statistic CD. In our case with $k = 8$ system configurations to compare and $N = 6$ measurements the critical value for a 90% of confidence is $CD = 1.83$. See an illustration of the resulting interval in Fig. 10. As the ranking of the ADA method does not intersect with the remaining system configurations ranks for that value of the CD, we can state that the ADA method outperforms the rest of the methods in the presented experiments. On the other hand, the best performance is obtained by the ADA method with SVM classifier. However, even if ADA SVM is the best method, the rank of this method intersects with ADA Adaboost, and thus, we cannot claim statistical significant differences between these two classifiers.

5. Discussion

5.1. Technical considerations

This paper presents and validates several contributions in the definition of a fully automatic system for ADHD diagnostic test. To our knowledge, this is the first automatic system for ADHD diagnosis present in the literature. The system contains three steps. In the first step, we apply the previously proposed CaudateCut to obtain an external segmentation of the caudate nucleus in MRI, which was previously validated. In the second step, we define a new automatic method for internal segmentation of the caudate nucleus in the head and body areas, learning a classifier based on an extended set of shape features describing the caudate region for each slice. These new features extend the geometric criterion defined by the ROI height and width relationship and include information of area, perimeter, orientation and position of the ROI. It is important to emphasize that this method avoids using external references, as caudate neighbor structures or anterior and posterior commissures. This fact has two main advantages, the procedure is quicker and more robust, since these external landmarks are of low resolution, small, and thus, complex to localize and can be a potential source of errors. We obtained high rates of accuracy, sensitivity and specificity, and we improved the results compared with the automatic method based on geometric criterion. The high rate performance in the internal segmentation is crucial in the final step of the diagnostic test method, since the considered volumetric features benefit from the head and body division. In particular, for the third step, we present the new 3D Dissociated Dipoles features to describe volumetric relations between left and right head and body areas of the caudate and build an automatic system learning the SVM classifier based on these new features. As we show in the results, the 3D Dissociated Dipoles features are simple but efficient, which obtain accurate results in discriminating ADHD subjects from control subjects in comparison to other standard and recent state-of-the-art volume descriptors. The proposed automatic ADHD diagnostic test obtains the best performance, even improving the previously proposed manual strategy based on the measure of a significant volumetric ratio. This improvement implies not only that this classifier offers better performance than the rest, but also that the new features offer additional information than the ratio itself, improving the discrimination power in the final ADHD diagnostic test.

An interesting point in the case of Adaboost classifier is that this classifier simultaneously performs feature selection while learning, and thus, we can analyze which features improve generalization in our data set, if necessary. We found that the ratio feature r_0 (Eq. (2)) is selected as the first choice by Adaboost in one fold and as the second choice in the remaining folds. These findings are in accordance with the morphological hypothesis stressed in [13] which states that the right caudate body is significantly smaller.

5.2. Contribution of each novelty

Each one of the novelties presented in this paper contributes to different aspects and in different ways to reach the final system performance:

- The combination of the extended new shape features with SVM and application of DS gives better results than for the automatic version of the state-of-the-art geometric criterion method.
- The small range of values of the ratio between ROI height and width (Eq. (1)) defined in the geometric criterium is an important source of false positives and false negatives. The number of false positives and negatives has been minimized using our new shape features, which add among others, information of area, perimeter, orientation and position of the ROI.
- The DS helps to define a proper internal boundary, and it has been proven to improve the classification rate.
- Manual and automatic ROC-based diagnostic test based on the ratio defined in Eq. (2) give poorer results compared with the approaches based on machine learning classification techniques and the new extended set of features.
- The new DD features improve the results obtained by other state-of-the-art feature extraction methods (GHKS and GDD).
- The internal segmentation of caudate nucleus is crucial for the definition of DD features, since the selection of GDD without considering head and body areas diminishes the performance.
- It is generally accepted that two of the most useful classifier methods are Adaboost and SVM. In general, both give good performances in binary classification and there is no theoretic justification to choose one over the other. We selected Adaboost as an example of an ensemble classifier approach and SVM as a well known binary-classifier. Between them, SVM gave the best results for the diagnostic test.

- Statistical significance tests are in general based on the performance of a method over several databases or performance of several methods over the same database. In our case, the Nemenyi statistical test was performed comparing eight different methods for ADHD diagnosis based on three measures (accuracy, sensitivity and specificity) over URNC database. The conclusion is that ADA method is statistically more significant than GHKS and GDD methods, although no significant differences are found between classifiers (Adaboost and SVM).
- The diagnostic power of the proposed fully automatic strategy is practical and reliable, since it highly replicates the performance of the manual diagnostic test and improves the results of the manual method previously presented.

5.3. Clinical considerations

Although DSM-IV-TR (American Psychiatric Association, 2000) provides a well-structured criteria based diagnosis, distinguishing ADHD from normal developmental levels of inattention, impulsivity and hyperactivity remains problematic. Further complications arise in integrating diagnostic data from different informants (e.g., parents and teachers; parents and children) and different settings (e.g., school, home). In these circumstances, a reliable ancillary test with high diagnostic accuracy is called for. Optimally, this test should have a good diagnostic performance, be well grounded in the previous ADHD research and allow for easy implementation in a clinical setting. The proposed automated MRI-based diagnostic test has a good diagnostic performance as a result of its relative high specificity. Given a prevalence of 10% of the ADHD in the general pediatric population [1], the negative predictive value approaches 95%. Therefore a negative result lowers dramatically the probability of an ADHD positive diagnosis. It is well grounded in the previous ADHD neuroimaging research, as it relies on caudate volumetric abnormalities that have been widely replicated in morphometric MRI studies in ADHD samples. Finally, it is fully automated, with a quick and easy post processing of the T1 weighted MRI images.

6. Conclusion

We presented a complete automatic method to assist in the diagnosis of ADHD. We were inspired by previous findings based on the caudate nucleus anatomy differentiating ADHD and control samples in the pediatric population. The proposed approach consists of three steps: (1) external caudate segmentation using the recently proposed CaudateCut segmentation algorithm, (2) a novel internal caudate segmentation of caudate head and body regions, and (3) a novel ADHD diagnostic test, being steps (2) and (3) the main novelties. For steps (2) we defined a novel classifier system based on shape features at slice level and for step (3) we learned a classifier to discriminate ADHD and control subject based on new 3D Dissociated Dipoles features. We performed separated validation processes of steps (2) and (3) in real data, obtaining high percentages of coincidences with manual annotations in both cases and showing important improvements with respect to state-of-the-art methods. The proposed diagnostic test method can detect subtle differences in the caudate nuclei between children with ADHD and controls, and provides significant predictive power for group membership. Moreover, it significantly improves diagnostic performance of the previously proposed manual strategy. Thus, we conclude that this work represents a key step towards the definition of a reliable and feasible automatic method to assist in the diagnosis of ADHD.

Future work will be devoted to study system evidences to classify symptom severity. We would like to study if there is a correlation between the distance from the separating hyperplane of the SVM and symptom severity. Furthermore, the method could be easily adapted to images acquired from different MRI scanners, after proper normalization of the data. So, we will compile new cases and apply the proposed diagnostic test to them. In order to extend the system to be applied to other range of ages, the system should be retrained using examples of those populations. That is also part of our future work.

Conflict of interest

The authors confirm their authorship and declare that they have no conflict of interest.

Acknowledgments

This work has been supported in part by projects TIN2009-14404-C02 and CONSOLIDER INGENIO CSD 2007-00018. We would like to thank Umberto Castellani for providing us the code of GHKS feature extraction.

Appendix A. Supplementary data

Supplementary data associated with this article can be found, in the online version, at http://dx.doi.org/10.1016/j.compmedimag.2012.08.002.

References

[1] Biederman FJ. Attention-deficit/hyperactivity disorder. Lancet 2005;366:237–48.
[2] Jensen PS. Current concepts and controversies in the diagnosis and treatment of attention deficit hyperactivity disorder. Curr Psychiatry Rep 2000;2(2):102–9.
[3] Soliva JC. Neuroimaging in the diagnosis of ADHD: where we are and where we are going. Expert Opin Med Diagn 2011;5(4):307–18, http://dx.doi.org/10.1517/17530059.2011.577413.
[4] Trèmols V, Bielsa A, Soliva JC, Raheb C, Carmona S, Tomàs J, et al. Tobeña, A. Bulbena, O. Vilarroya, Differential abnormalities of the head and body of the caudate nucleus in attention deficit-hyperactivity disorder. Psychiatric Research 2008;163(3):270–8.
[5] Seidman LJ, Valera EM, Makris N. Structural brain imaging of attention-deficit/hyperactivity disorder. Biol Psychiatry 2005;57(11):1263–72.
[6] Soliva JC, Vilarroya O. Aportaciones de la resonancia magnetica estructural al esclarecimiento de la neurobiologia del trastorno por deficit de atencion/hiperactividad: hacia la identificacion de un fenotipo neuroanatomico. Rev Neurol 2009;48(11):592–8.
[7] Valera EM, Faraone SV, Murray KE, Seidman LJ. Meta-analysis of structural imaging findings in attention-deficit/hyperactivity disorder. Biol Psychiatry 2007;61(12):1361–9.
[8] Castellanos F, Giedd J, Eckburg P, Marsh W, Vaituzis A, Kaysen D, et al. Quantitative morphology of the caudate nucleus in attention deficit hyperactivity disorder. Psychiatry 1994;151:1791–6.
[9] Castellanos F, Giedd J, Marsh W, Vaituzis A, Kaysen D, adn SH, et al. Quantitative brain magnetic resonance imaging in attention-deficit hyperactivity disorder. Arch Gen Psychiatry 1996;53(7):607–16.
[10] Castellanos FX, Giedd JN, Berquin PC, Walter JM, Sharp W, Tran T, et al. Quantitative brain magnetic resonance imaging in girls with attention-deficit/hyperactivity disorder. Arch Gen Psychiatry 2001;58(3):289–95.
[11] Castellanos FX, Lee PP, Sharp W, Jeffries NO, Greenstein DK, Clasen LS, et al. Developmental trajectories of brain volume abnormalities in children and adolescents with Attention-Deficit/Hyperactivity Disorder. J Am Med Assoc 2002;288(14):1740–8, http://dx.doi.org/10.1001/jama.288.14.1740.
[12] Pineda DA, Restrepo MA, Sarmiento RJ, Gutierrez JE, Vargas SA, Quiroz YT, et al. Statistical analyses of structural magnetic resonance imaging of the head of the caudate nucleus in Colombian children with attention-deficit hyperactivity disorder. J Child Neurol 2002;17(2):97–105, http://view.ncbi.nlm.nih.gov/pubmed/11952084.
[13] Soliva JC, Fauquet J, Bielsa A, Rovira M, Carmona S, Ramos-Quiroga JA, et al. Quantitative MR analysis of the caudate abnormalities in pediatric ADHD: proposal for a diagnostic test. Psychiatric Res: Neuroimaging 2010;182(3):238–43.
[14] Boutros N, Fraenkel L, Feingold A. A four-step approach for developing diagnostic tests in psychiatry: EEG in ADHD as a test case. J Neuropsychiatry Clin Neurosci 2005;17(4):455–64, http://dx.doi.org/10.1176/appi.neuropsych.17.4.455.
[15] Igual L, Soliva JC, Hernandez-Vela A, Escalera S, Jimenez X, Vilarroya O, Radeva P. A fully-automatic caudate nucleus segmentation of brain MRI: application in pediatric attention-deficit/hyperactivity disorder volumetric analysis. BioMed Eng Online 2011;10(105), doi:10.1186/1475-925X-10-105.

[16] Cuingnet R, Gerardin E, Tessieras J, Auzias G, Lehéricy S, Habert M-OO, et al. Automatic classification of patients with Alzheimer's disease from structural MRI: A comparison of ten methods using the ADNI database. NeuroImage 2011; doi:10.1016/j.neuroimage.2010.06.013.
[17] Heckemann RA, Keihaninejad S, Aljabar P, Gray KR, Nielsen C, Rueckert D, et al. Automatic morphometry in Alzheimer's disease and mild cognitive impairment. NeuroImage 2011; doi:10.1016/j.neuroimage.2011.03.014.
[18] Wolz R, Heckemann RA, Aljabar P, Hajnal JV, Hammers A, Lötjönen J, et al. Measurement of hippocampal atrophy using 4D graph-cut segmentation: application to ADNI. NeuroImage 2010;52(1):109–18, http://dx.doi.org/10.1016/j.neuroimage.2010.04.006.
[19] Qiu A, Fennema-Notestine C, Dale AM, Miller MI. Regional shape abnormalities in mild cognitive impairment and Alzheimer's disease. NeuroImage 2009;45(3):656–61, http://dx.doi.org/10.1016/j.neuroimage.2009.01.013.
[20] Frisoni GB, Fox NC, Jack CR, Scheltens P, Thompson PM. The clinical use of structural MRI in Alzheimer disease. Nature Reviews Neurology 2010;6(2):67–77, http://dx.doi.org/10.1038/nrneurol.2009.215.
[21] Weiner MW, Aisen PS, Jack CR, Jagust WJ, Trojanowski JQ, Shaw L, et al. The Alzheimerś disease neuroimaging initiative: progress report and future plans. Alzheimers Dementia J Alzheimers Assoc 2010;6(3), 202-11.e7.
[22] Ecker C, Marquand A, Mour ao Miranda J, Johnston P, Daly EM, Brammer MJ, et al. Describing the brain in autism in five dimensions-magnetic resonance imaging-assisted diagnosis of autism spectrum disorder using a multiparameter classification approach. J Neurosci 2010;30(32):10612–23.
[23] Ecker C, Rocha-Rego V, Johnston P, Mourao-Miranda J, Marquand A, Daly EM, et al. Investigating the predictive value of whole-brain structural MR scans in autism: a pattern classification approach. Neuroimage 2010;49(1):44–56.
[24] Costafreda SG, Chu C, Ashburner J, Fu CHY. Prognostic and diagnostic potential of the structural neuroanatomy of depression. PLoS One 2009;4(7):e6353.
[25] Hahn T, Marquand AF, Ehlis A-CC, Dresler T, Kittel-Schneider S, Jarczok TA, et al. Integrating neurobiological markers of depression. Arch Gen Psychiatry 2010, http://dx.doi.org/10.1001/archgenpsychiatry.2010.178.
[26] Fan Y, Shen D, Gur RC, Gur RE, Davatzikos C, Compare. Classification of morphological patterns using adaptive regional elements. IEEE Trans Med Imaging 2007;26(1):93–105.
[27] Shenton ME, Dickey CC, Frumin M, McCarley RW. A review of MRI findings in schizophrenia. Schizophrenia Res 2001;49(1-2):1–52.
[28] Gerig G, Styner M, Jones D, Weinberger D, Lieberman J. Shape analysis of brain ventricles using SPHARM. In: IEEE workshop on mathematical methods in biomedical image analysis. 2001. p. 171–8, http://dx.doi.org/10.1109/MMBIA.2001.991731.
[29] Toews M, Collins D, Arbel T. Feature-based morphometry: Discovering group-related anatomical patterns. Neuroimage 2010;49(3):2318–27.
[30] Castellani U, Mirtuono P, Murino V, Bellani M, Rambaldelli G, Tansella M, et al. A new shape diffusion descriptor for brain classification. MICCAI 2011;2:426–33.
[31] Bronstein MM, Bronstein AM. Shape recognition with spectral distances. IEEE Trans Pattern Anal Mach Intell 2011;33(5):1065–71.
[32] Wels M, Zheng Y, Huber M, Hornegger J, Comaniciu D. A discriminative model-constrained EM approach to 3D MRI brain tissue classification and intensity non-uniformity correction. Phys Med Biol 2011;56(11):3269.
[33] Kolmogorov V, Zabih R. What energy functions can be minimized via graph cuts. PAMI 2004;26:65–81.
[34] Talairach J, Tournoux P. Co-planar stereotaxic atlas of the human brain: 3-dimensional proportional system—an approach to cerebral imaging. Thieme Medical Publishers; 1988.
[35] Ai WI, Langley P. Induction of one-level decision trees. In: Proceedings of the ninth international conference on machine learning. 1992. p. 233–40.
[36] Reyzin L, Schapire R. How boosting the margin can also boost classifier complexity. In: Proceedings of the 23rd international conference on Machine Learning. 2006. p. 753–60.
[37] Balas BJ, Sinha P. Dissociated dipoles: image representation via non-local comparisons. In: CBCL Paper 229/AI Memo 2003-018, Massachusetts Institute of Technology. MIT Press; 2003.
[38] Baró X, Vitrià J. Weighted dissociated dipoles: an extended visual feature set. ICVS 2008:281–90.
[39] Van den Bergh M, Koller-Meier E, Van Gool L. Real-time body pose recognition using 2D or 3D Haarlets. Int J Comput Vis 2009; doi:10.1007/s11263-009-0218-0.
[40] Morra JH, Tu Z, Apostolova LG, Green AE, Avedissian C, Madsen SK, et al. Validation of a fully automated 3D hippocampal segmentation method using subjects with Alzheimer's disease mild cognitive impairment, and elderly controls. NeuroImage 2008;43(1):59–68, http://dx.doi.org/10.1016/j.neuroimage.2008.07.003.
[41] Monno L, Bellotti R, Calvini P, Monge R, Frisoni G, Pievani M. Hippocampal segmentation by random forest classification. In: IEEE International Workshop on Medical Measurements and Applications Proceedings (MeMeA). 2011., http://dx.doi.org/10.1109/MeMeA.2011.5966763.
[42] Viola P, Jones M. Robust real-time object detection. Int J Comput Vis 2001:137–54.
[43] Friedman J, Hastie T, Tibshirani R. Additive logistic regression: a statistical view of boosting (with discussion and a rejoinder by the authors). Ann Stat 2000;28(2):337–407.
[44] Dietterich TG. Approximate statistical tests for comparing supervised classification learning algorithms. Neural Comput 1998;10:1895–923.
[45] Demsar J. Statistical comparisons of classifiers over multiple data sets. JMLR 2006;7:1–30.
[46] Iman RL, Davenport JM. Approximations of the critical region of the Friedman statistic. Commun Stat 1980:571–95.

Laura Igual received the degree in Mathematics from Universitat de Valencia in 2000. She studied at Université de Liège (Belgium) for a year. She developed her Ph.D Thesis in Computer Science and Digital Communication in the Department of Technology of the Universitat Pompeu Fabra, partially supported by the French Centre National d'Etudes Spatiales (CNES) and the company THALES (France). She obtained her Ph.D Thesis in January 2006 and since then she is a research member at the Computer Vision Center of the Universitat Autònoma de Barcelona. Since 2009, she is also a lecturer at Department of Mathematics at Universitat de Barcelona. She is a member of the Perceptual Computing Group and a consolidated research group of Catalonia and her research interests focus on medical imaging.

Joan Carles Soliva is an MD and PhD neuroradiologist who works as a researcher at the Cognitive Neuroscience Unit (URNC) at Department of Psychiatry of the Universitat Autònoma de Barcelona, Spain, and the Neuroimaging Research Group (NRG), at the Fundació IMIM, Barcelona, Spain. Both groups have the objective of applying neuroimaging techniques to the study of cognitive functions, and have been consolidated as leaders in the study of brain abnormalities in different child and adult psychiatry conditions. He has also been working as a consultant neuroradiologist at several university hospitals in Barcelona. As a researcher, he has been mainly focused in ADHD and published in the field of neuroimaging of psychiatric disorders.

Sergio Escalera received the BS and MS degrees from the Universitat Autònoma de Barcelona (UAB), Barcelona, Spain, in 2003 and 2005, respectively. He obtained the PhD degree on Multi-class visual categorization systems at Computer Vision Center, UAB. He obtained the 2008 best Thesis award on informatics at Universitat Autònoma de Barcelona. He is a lecturer of the Department of Applied Mathematics and Analysis, Universitat de Barcelona. He is a partial time professor at Universitat Oberta de Catalunya. He is a member of the Perceptual Computing Group and a consolidated research group of Catalonia. He is also a member of the International Foundation of Research & Analysis. He is an editorial board member of Journal of Convergence Section C: Web and Multimedia.

Roger Gimeno received the BS degree from the Universitat Politecnica de Catalunya (UPC), Barcelona, Spain, in 2010 and MS degree from the Universitat Autònoma de Barcelona (UAB), Barcelona, Spain, in 2011. Currently, he is R+D Engineer in ICAR Vision Systems.

Oscar Vilarroya is an MD and PhD who heads the Cognitive Neuroscience Unit (URNC) at Department of Psychiatry of the Universitat Autònoma de Barcelona, Spain, and the Neuroimaging Research Group (NRG), at the Fundació IMIM, Barcelona Spain. Both groups have the objective of applying neuroimaging techniques to the study of cognitive functions, and have been consolidated as leaders in the study of brain abnormalities in different child and adult psychiatry conditions. As a researcher, he has published studies in the field of neuroimaging of psychiatric diseases, as well as in the domain of cognitive science and neurobiology.

Petia Radeva is a researcher at the University of Barcelona. She received the PhD at Universitat Autònoma de Barcelona in 1998. She has more than 150 publications in high impact factor journals and international conferences in the field of Computer Vision. She supervised more than 15 national and international research and transfer projects. She has 12 patents in the field of medical imaging. She is actually supervising projects in the field of cardiac imaging and wireless endoscopic in collaboration with Spanish hospitals and international companies related to medical imaging.